RSC Advances




ROYAL SOCIETY OF CHEMISTRY

www.rsc.org/advances

# A novel Cu-Mn/Ca-Zr catalyst for the synthesis of methyl formate from syngas

Haijun Zhao[a, b], Minggui Lin[a, *], Kegong Fang[a], Juan Zhou[a], Ziyu Liu[c], Gaofeng Zeng[c], Yuhan Sun[c, *]

[a] State Key Laboratory of Coal Conversion, Institute of Coal Chemistry, Chinese Academy of Sciences, Taiyuan 030001, Shanxi, P.R. China

[b] University of Chinese Academy of Sciences, Beijing, 100049, P.R. China

[c] Key Laboratory of Low-carbon Conversion Science and Engineering, Shanghai Advanced Research Institute, Chinese Academy of Sciences, Shanghai, 201203, P.R. China

**Abstract**

Cu-Mn mixed oxides and mesoporous CaO-$ZrO_2$ solid base were prepared by complexing method and alcohothermal route, respectively, and they were mixed together as combined Cu-Mn/Ca-Zr catalyst which was evaluated for the direct synthesis of methyl formate (MF) from syngas in a slurry reactor. Cu-Mn and CaO-$ZrO_2$ samples were characterized by $N_2$ isotherm adsorption-desorption, XRD, SEM, TEM, XPS and $CO_2$-TPD techniques. Under the optimum reaction conditions of 160 $^oC$, 3 MPa, 3:7 for the ratio of methanol to N, N dimethylformamide, 40 g $L^{-1}$ for Cu-Mn sample, and 30 g $L^{-1}$ for CaO-$ZrO_2$ sample, a lower CO conversion of 22.4 % was obtained over Cu-Mn/Ca-Zr, whereas the MF selectivity of 82.3% was higher than that of traditional catalyst (e.g. Cu-catalyst and $NaOCH_3$), which was due to the synergism between Cu-Mn and CaO-$ZrO_2$ samples.

* Corresponding authors.

E-mail address: linmg@sxicc.ac.cn (Minggui, Lin), yhsun@sxicc.ac.cn (Yuhan, Sun)

## 1. Introduction

Methyl formate (MF) is one of the most important chemical intermediates, which can be used to synthesize a large number of chemicals such as formic acid, acetic acid, ethylene glycol, methyl propionate and methyl glycolate.[1-5] Besides, MF is considered to be a promising substitute for methyl tertiary butyl ether (MTBE) and ecological fuel for vehicles.[6,7] In agriculture, MF is regarded as pesticide, bactericide and fruit desiccant. Thus, the catalytic synthesis of MF has attracted much attention of researchers.

There are many effective processes developed for MF synthesis so far. The commercial method to synthesize MF is the carbonylation of methanol over alkali methoxide catalysts at 80 $^{o}$C in liquid phase[8-10]. However, the catalyst deactivation caused by $CO_2$ and $H_2O$ in system exist in above process. Recently, the selective oxidation of methanol to MF on noble metal catalysts such as Au, Ru, Ag and Pd has been the research hotspot due to its high conversion and selectivity.[11-15] Wojcieszak et al.[16] studied the oxidation of methanol to methyl formate over Pd nanoparticles supported on $\gamma$-$Fe_2O_3$ at 80 $^{o}$C with 76% methanol conversion and 81% MF selectivity. Wang et al.[17] reported methanol selective oxidation, with a methanol conversion of 90.2% and selectivity of 100% to methyl formate, at 70 $^{o}$C on graphene-supported Au-Pd nanoparticles, owing to the synergism of Au and Pd particles as well as the strong interaction between graphene and Au–Pd nanoparticles. The major disadvantage of this process is the cost of catalyst due to the presence of noble metal. Besides, the photocatalytic reduction of $CO_2$ to MF in methanol also aroused the interests of researchers.[18,19] Chen et al.[20,21] employed the photocatalytic reduction of $CO_2$ to MF on $B_2S_3$ and Ni-doped ZnS catalyst with the rate of MF production 175

μmol $g^{-1}$ $h^{-1}$ and 121 μmol $g^{-1}$ $h^{-1}$, respectively, while the low yield and poor stability limit the application of this process. This has stimulated a desire for the development of an alternative process.

Direct synthesis of MF from syngas in liquid-phase system is significantly concerned by researchers due to its atomic economy and short reaction process.[22-26] The direct process follows the stoichiometry: $2CO+2H_2 \rightarrow HCOOCH_3$, $\Delta H_0^R$ = -157.2 kJ $mol^{-1}$ (1).[27] In the direct synthesis process, MF formed as an intermediate of methanol synthesis from syngas on mixed catalyst comprised of alkali or alkali earth compounds and Cu-based catalysts,[22] which contains homogeneous carbonylation of methanol on alkali or alkali earth compounds and heterogeneous hydrogenation of MF on Cu-based catalysts. Palekar et al.[23] controlled the selectivity of methanol and MF by changing reaction temperature and the ratio of CO to $H_2$. They found that high reaction temperature and low $CO/H_2$ were beneficial to methanol; on the contrary, low reaction temperature and high $CO/H_2$ condition favored MF formation, and the similar results were also reported by Chen et al.[28] However, a critical problem in this process is that homogeneous alkali or alkali earth compounds is susceptible to $CO_2$ or $H_2O$ in reaction system, which accelerate the fall of the catalytic activity.[29-31] Moreover, alkali or alkali earth compounds distributed on the surface of Cu-based catalyst caused the blockage of active sites.[32]

In this work, $CaO-ZrO_2$ solid base and Cu-Mn mixed oxides were prepared and characterized by $N_2$ isotherm adsorption-desorption, XRD, TEM, SEM, XPS and $CO_2$-TPD measurements. More importantly, the combined Cu-Mn/Ca-Zr catalyst prepared by mechanical mixing above two as-prepared samples was applied to the direct synthesis of MF from syngas in a batch slurry reactor for the first time. In addition, the influences of reaction parameters such as temperature, pressure, the ratio

of methanol to DMF, the concentration of $CaO-ZrO_2$ and Cu-Mn smaples on catalytic performance were thoroughly investigated.

## 2. Experimental

### 2.1 Preparation of catalysts

#### 2.1.1 Preparation of Cu-Mn mixed oxides

The preparation of Cu-Mn mixed oxides is described as follows: 1 M $Mn(NO_3)_2$ aqueous solution with pH = 3-4 was dropped into 1 M copper ammonia solution of pH = 9-10 with vigorous stirring at 35 °C at a dropping rate of 1mL $min^{-1}$. After aging for 5 h, the precipitate was washed with deionized water for several times, then filtered, dried, and calcined at 550 °C for 4 h. The normal molar ratio of Cu to Mn was 1.0.

#### 2.1.2 Preparation of $CaO-ZrO_2$ solid base

$CaO-ZrO_2$ solid base was prepared by sol-gel method as the reported procedure previously.[33] Typically, 1 g of amphiphilic poly block copolymers ($PEO_{20}PPO_{70}PEO_{20}$, Pluronic P123, Aldrich) and 1.5 g $Ca(NO_3)_2 \cdot 4H_2O$ were dissolved in 24.2 mL absolute ethanol, which noted as solution A. Meanwhile, 4 g of zirconium n-propoxide (70 wt. % in n-propanol, Alfa Aesar) and 0.43 g acetylacetone were dissolved in 16.1 mL absolute ethanol to produce solution B. Then solution B and 1.6 mL $H_2O$ were dropped slowly into solution A sequentially. The resulting solution was stirred for 2 h before it was aged at 60 °C for 24 h. After aging, the acquired white gel was refluxed in 0.5 M NaOH solution for 24 h. Subsequently, the product was washed by deionized water to remove residual $Na^+$ and filtered. The white hybrid was then dried at 100 °C overnight and calcined at 600 °C for 6 h to produce solid base, and the normal mole

ratio of Ca to Zr is 0.5.

### 2.1.3 Preparation of Cu-Mn/Ca-Zr catalyst

Cu-Mn/CaO-$ZrO_2$ combined catalyst, noted as Cu-Mn/Ca-Zr, was prepared by mechanical mixing Cu-Mn mixed oxides and CaO-$ZrO_2$ solid base. The mass ratio of Cu-Mn to CaO-$ZrO_2$ is determined by the concentration of two samples in slurry phase. The concentration of Cu-Mn catalyst is 0-65 g $L^{-1}$, and that of CaO-$ZrO_2$ catalyst is 0-50 g $L^{-1}$.

### 2.2 Catalyst characterization

The specific surface area of the sample was measured with ASAP 2020 analyzer using the multipoint Brunauer, Emmett and Teller (BET) adsorption. X-ray diffraction (XRD) characterization including small-angle (SXRD) was conducted using a Bruker diffractometer employing Cu Kα radiation (40 kV and 40 mA). Scanning electron microscopy (SEM) images were taken with a JSM-7001F electron microscope operating at 10 or 5 kV. Transmission electron microscopy (TEM) images were recorded using a JEM-2100F microscope operated at 200 kV. X-ray photoelectron spectroscopy (XPS) experiments were carried out with an AXIS ULTRA DLD X photoelectron spectrometry employing an Al-Kα X-ray source. The binding energy of the samples was corrected with the energy of C1s (284.6 eV) as the reference. Temperature-programmed desorption of $CO_2$ ($CO_2$-TPD), 0.2 g samples were pretreated in a flow of He (99.99%) at a rate of 10 $^oC$ $min^{-1}$ from room temperature to 700 $^oC$ and kept for 2 h. Prior to adsorption of $CO_2$ (99.999%) at 30 $^oC$, blank experiment was carried out from 30 $^oC$ to 700 $^oC$ to confirm no $CO_2$ desorption occurred. When the temperature elevated, the $CO_2$ desorbed was detected by TCD.

### 2.3 Catalyst performance testing

A batch stainless steel autoclave reactor with an inner volume of 100 mL was employed. The designed amount of Cu-Mn/Ca-Zr catalyst and solvent including methanol (99.95%) and N, N dimethyl formamide (99.5%, DMF) were poured into the reactor. After replacing the air in reactor with $N_2$ for 2-3 times, feed gas was permitted into the reaction system at room temperature until the pressure of the system increased to the required level. Then the temperature was increased in 30 min. The stirring speed was 1000 rpm to resist mass transfer effect. The gas phase was analyzed using Carbosieve-packed column equipped with thermal conductivity detector (TCD) and Porapack-Q column equipped with flame ionization detector (FID), and liquid samples were analyzed on Porapack-T column equipped with thermal conductivity detector (TCD). The composition of the feed gas is $H_2/CO/N_2 =$ 64/32/4, where nitrogen was employed as an internal standard.

## 3. Results and discussion

### 3.1 Catalyst characterization

#### 3.1.1 Physicochemical properties

Fig. 1 shows the $N_2$ isotherm adsorption-desorption and pore size distribution (inserted) profiles of CaO-$ZrO_2$. As can be seen, the CaO-$ZrO_2$ solid base shows the type IV isotherm and H2 hysteresis loop. The presence of type IV isotherm plot indicates the mesoporous structure of CaO-$ZrO_2$, and H2 hysteresis loop is the characteristic of "ink-bottle" or "network" type of pores formed from the voids between nano-particles in this sample.[34] Meanwhile, the CaO-$ZrO_2$ sample exhibits an narrow pore size distribution ranging from 1.8 nm to 10 nm with a center at 3.7 nm in the inserted of Fig. 1, suggesting a rather uniform pore structure of CaO-$ZrO_2$. The

SXRD plot of $CaO-ZrO_2$ shows a broad peak with maximum at $1.28^o$ (Fig. 2), which indicates the uniform pore structure of $CaO-ZrO_2$ in line with the result of Fig.1. Besides, the $CaO-ZrO_2$ possesses a specific surface area of 53 $cm^2\ g^{-1}$ determined by BET surface area. However, the Cu-Mn catalyst with a very small specific surface area of 14 $cm^2\ g^{-1}$ is obtained.

### 3.1.2 XRD measurements

The crystalline phases of $CaO-ZrO_2$ and Cu-Mn oxide samples are investigated by XRD analysis (Fig. 3). For the $CaO-ZrO_2$ solid base, only tetragonal $ZrO_2$ (PDF 88-1007) diffraction peaks at $30.3^o$, $35.2^o$, $50.6^o$ and $60.3^o$ are detected, while no peaks belonging to CaO are found, which indicates that CaO is highly dispersed in solid base with amorphous structure, or $Ca^{2+}$ incorporates in $ZrO_2$ lattice and homogeneous $CaO-ZrO_2$ solid solution is formed.[35,36] The diffraction peaks of $CaO-ZrO_2$ are broad and weak, which implies that the $CaO-ZrO_2$ solid base possesses very small crystalline size or low crystallinity. For the Cu-Mn mixed oxides, CuO (Tenorite, PDF 72-0629) and incomplete spinel $Cu_{1.5}Mn_{1.5}O_4$ (PDF 70-0262) with monoclinic and cubic structures are observed, and no diffraction peaks corresponding to Mn oxides are detected, which is due to partial Mn species existing in amorphous or being in highly dispersed.

### 3.1.3 SEM and TEM

The morphology information of Cu-Mn and $CaO-ZrO_2$ catalysts is characterized by SEM in Fig. 4a and b. The Cu-Mn is mainly comprised of uniform particles with the size of 50-100 nm, which aggregate together in random (Fig. 4a). For the $CaO-ZrO_2$ catalyst, both large lumps (≈10 μm) with flat surfaces and smaller particles on top are

observed, which might be formed from the clusters of primary particles (See Fig. 4d).

TEM is used to investigate the particle size and textural structure of Cu-Mn and $CaO\text{-}ZrO_2$ samples (Fig. 4c-f). As shown in Fig. 4c, the Cu-Mn exhibits loose agglomerates with the particle size about 20-100 nm. The lattice spacings of 0.27 nm and 0.21 nm could be assigned to the (110) planes of CuO and (400) planes of $Cu_{1.5}Mn_{1.5}O_4$ as given in Fig. 4e, which indicates the coexistence of CuO and $Cu_{1.5}Mn_{1.5}O_4$ phases in Cu-Mn mixed oxides, in line with the result of XRD (Fig. 3b). The $CaO\text{-}ZrO_2$ is highly porous in nature and consists of the narrowly distributed nanoparticles with the size less than 10 nm (Fig. 4d). It can be seen in Fig. 4f that nano-crystals and amorphous nano-particles are coexistence in $CaO\text{-}ZrO_2$ sample, indicating that $CaO\text{-}ZrO_2$ is semi-crystalline structure, in accordance with the weak and broad diffraction peak in XRD pattern (Fig. 3a).

### 3.1.4 XPS measurements

The oxidation states of Cu and Mn component in Cu-Mn catalyst are determined via XPS surface analysis (Fig. 5). Five peaks are distinguished by deconvoluting Mn 2p peak. The peak at 641.1 eV and 652.9 eV are attributed to $Mn^{2+}$ and the peak at 642.7 eV and 654.4 eV are assigned to $Mn^{3+}$ or $Mn^{4+}$ cations.[37,38] Moreover, a satellite peak at 648.2 eV could be detected, which suggests the presence of $Mn^{2+}$.[39-41] However, there are no $Mn^{2+}$ oxide peaks in XRD patterns (Fig. 3), indicating that the $Mn^{2+}$ oxides coexist in amorphous structure with $Cu_{1.5}Mn_{1.5}O_4$ and CuO in Cu-Mn sample.

From the Cu 2p XPS plot of Cu-Mn catalyst (Fig. 5b), it can be seen that Cu $2p_{3/2}$ main peaks located at 933.7 eV and 934.9 eV which are assigned to $Cu^{2+}$ species. The shake-up satellite peaks at 941.4 eV and 943.8 eV corresponding to Cu $2p_{3/2}$ also

confirm the presence of $Cu^{2+}$, and these peaks do not appear in $Cu^{+}$ or $Cu^{0}$ species, since shake-up transitions do not occur in filled 3d shells and metallic states.[41,42] The Cu 2p XPS profile also shows a peak at the binding energy of 930.9 eV, which could be attributed to cuprous or metallic copper.[40,42] Unfortunately, $Cu^{0}$ cannot be clearly distinguished from $Cu^{+}$ by the XPS profile of Cu 2p due to their similar position of binding energy. It is reported that the following redox equilibrium is established in $Cu_{1.5}Mn_{1.5}O_4$,[40-43] $Cu^{2+} + Mn^{3+} = Cu^{+} + Mn^{4+}$. Therefore, it can be assumed that the peak at 930.9 eV is characteristic of $Cu^{+}$ cation. Auger electron spectroscopy is taken to further distinguish the chemical state between $Cu^{+}$ and $Cu^{0}$ (Fig. 6). According to the literatures,[40,44-45] the peak of Auger spectra with kinetic energy of 918.5 eV is assigned to $Cu^{0}$, the peak at 917.6 eV, which is attributed to $Cu^{2+}$, for the peak at 916.5 eV, which is related to $Cu^{+}$. In this case, the corresponding kinetic energy spectra of Auger electron includes two peaks at 917.8 eV and 916.8 eV (Fig. 6), which could be assigned to $Cu^{2+}$ and $Cu^{+}$. Besides, a low kinetic energy broad peak at 913.1 eV can be observed, which belongs to $Cu^{2+}$ or $Cu^{+}$ according to the literature,[46] indicating the absence of $Cu^{0}$. In addition, there is no possibility to form $Cu^{0}$ during the preparation process of Cu-Mn oxide, for the samples were calcined at 550 $^{o}$C in air, in line with the results of Mn 2p XPS and XRD.

### 3.1.5 $CO_2$-TPD

The $CO_2$ desorption temperature can be used to evaluate the base strength, and the basicity of each type of basic site is determined by the desorption amount of $CO_2$. As shown in Fig. 7, the basic property of CaO-$ZrO_2$ is characterized by $CO_2$-TPD. The $CO_2$ desorption profile can be roughly divided into three broad peaks: low temperature peak below 235 $^{o}$C, medium temperature peak from 240 $^{o}$C to 515 $^{o}$C and

high temperature peak around 603 $^{o}$C, which are named α, β and γ, respectively. The α peak centered at 163 $^{o}$C with about 62 μmol $g^{-1}$ $CO_2$ uptake could be assigned to the $CO_2$ desorption on the weak basic site of $ZrO_2$ surface. The β peak centered at 362 $^{o}$C with about 219 μmol $g^{-1}$ $CO_2$ uptake is related to the moderately strong basic site from the surface of a solid solution, in which the presence of neighboring $Ca^{2+}$ and $Zr^{4+}$ affect the basicity of lattice oxygen on the surface,[47] and the γ peak at 603 $^{o}$C with 42 μmol $g^{-1}$ $CO_2$ uptake is attributed to the strong basic site on the surface of CaO in CaO-$ZrO_2$.[33] It could be concluded from the results above that there are three basic sites with different basic strength on the CaO-$ZrO_2$ solid base surface, and the basicity of three basic sites follows β > α > γ.

### 3.2 Influence of reaction variables on MF synthesis

Slurry phase is a complex reaction system, and many factors can influence the catalytic activity and the selectivity of products. In the present work, reaction variables such as temperature, pressure, the ratio of methanol to DMF, the concentration of CaO-$ZrO_2$ and Cu-Mn samples have been investigated. To simplify the effect of other parameters, only one parameter is changed while others kept unchanged.

#### 3.2.1 Reaction temperature

The effect of reaction temperature on the catalytic performance of MF synthesis is given in Fig. 8. It can be seen that CO conversion monotonically increases with the rise of temperature from 140 °C to 200 °C. The space-time yield (STY) of MF is relatively low at 140 °C, while it sharply reaches a maximum value of 4.18 g $L^{-1}$ $h^{-1}$ at 160 °C and then decreases. The MF selectivity firstly increases from 29.3% to 83.5%

as the temperature rises from 140 °C to 160 °C, and then begins to decrease after further increasing the temperature. It can be inferred from equation (1) that the synthesis of MF from syngas is a strongly exothermal reaction. The reaction proceeds slowly at low temperature, which leads to a low CO conversion. However, the selectivity of MF reaches maximum at the low temperature of 160 °C and begins to decrease at higher temperature. Therefore, the reaction temperature of 160 °C is beneficial to the formation of MF. The selectivity of formaldehyde and ethanol shows the opposite trend to that of MF.

### 3.2.2 Reaction pressure

Equation (1) indicates that the reaction of MF synthesis from syngas is a gas volume reducing process before and after reaction. As a consequence, the process would be favorable to the conversion of CO at higher reaction pressure in a thermodynamics point view, and vice versa. The relationship between catalytic performance and initial pressure is shown in Fig. 9. With increasing the pressure, CO conversion firstly increases from 11.0% at 2 MPa to 20.2% at 3 MPa and then decreases slowly as the pressure increases above 3 MPa. This result seems to be opposite to the thermodynamic rule that higher pressure would make the balance move towards the side where the gas volume decreases, vice versa, which could be explained by the evaluation method of catalyst. In the present work, the amount of feed gas purged into the batch reactor at low pressure is less than that at high pressure, which leads to the phenomenon that the CO conversion at high pressure is smaller than that at low pressure. The monotonic rise of STY (MF) from 2.85 g $L^{-1}$ $h^{-1}$ at 2 MPa to 4.03 g $L^{-1}$ $h^{-1}$ at 6 MPa could also demonstrate that the process of MF synthesis follows the thermodynamic rule above. The selectivity of MF consistently

keeps about 80% with increasing pressure from 2 MPa to 6 MPa, indicating the little influence of reaction pressure on product selectivity.

### 3.2.3 The ratio of methanol to DMF

The polarity of solvent in this work is controlled by changing the volume ratio of methanol to DMF, and its influence on catalytic performance is listed in Table 1. As can be seen, CO conversion rises firstly and then declines with decreasing the ratio of methanol to DMF. The STY of MF reaches the maximum value of 4.18 g $L^{-1}$ $h^{-1}$ at the ratio of 3:7 and begins to decline with further decreasing the ratio. For selectivity, it can be seen that the MF selectivity firstly enhances with decreasing the ratio of methanol to DMF from 9:1 to 3:7 and then reaches a plateau level about 83.5%, whereas the selectivity of formaldehyde and ethanol substantially descend until the ratio of methanol to DMF decreases to 3:7. It is well-known that the polarity of methanol is higher than that of DMF, and the polarity of the liquid phase decreases with decreasing the ratio of methanol to DMF. Therefore, the appropriate polarity of solvent is indispensable for the high conversion of CO and STY of MF. The lower polarity of liquid phase is beneficial to the selectivity of MF, while the higher polarity of liquid phase supports the conversion of CO.[48] Moreover, methanol or DMF molecular in solvent could interact with products, which may also have a significant influence on CO conversion and MF selectivity.

### 3.2.4 The concentration of $CaO\text{-}ZrO_2$ or Cu-Mn catalysts

The influence of $CaO\text{-}ZrO_2$ concentration on catalytic performance is shown in Fig. 10. CO conversion drastically varies from 3.3% to 12.0% as the $CaO\text{-}ZrO_2$ concentration increases from 0 to 30 g $L^{-1}$. In this concentration range, the STY and

the selectivity of MF also enhance significantly from 0.28 g $L^{-1}$ $h^{-1}$ and 14.4% to 2.08 g $L^{-1}$ $h^{-1}$ and 72.4%, respectively, while the selectivity of formaldehyde and ethanol decreases. Further increasing the CaO-$ZrO_2$ concentration, its influence on CO conversion and selectivity could be ignored. The influence of Cu-Mn concentration on catalytic performance is shown in Fig. 11. CO conversion and MF selectivity firstly rise up to 12.2% and 74.2% as Cu-Mn concentration increases from 0 to 40 g $L^{-1}$, and subsequently reduce with further increasing Cu-Mn concentration. As for the STY of MF, it monotonically increases until the concentration is more than 55 g $L^{-1}$.

More active sites would be exposed with increasing the catalyst concentration, when the concentration of CaO-$ZrO_2$ or Cu-Mn catalysts increases below 30 g $L^{-1}$ and 40 g $L^{-1}$, leading to the increase of CO conversation and MF selectivity. However, as the concentration of CaO-$ZrO_2$ and Cu-Mn catalysts is higher than 30 g $L^{-1}$ and 40 g $L^{-1}$, the mass transfer resistance of system increases with further increasing the concentration of samples.[49] More specifically, the slurry dispersion of catalyst is defined and becomes worse; the apparent viscosity of system increases resulting in the decay of interface mobility, and the solubility of gas phase in slurry decreases. As a consequence of this, CO conversation and MF selectivity increase slowly or begin to decrease, and the reaction process might transfer to thermodynamics control from dynamics control.

### 3.3 Catalytic performance for MF synthesis

According to the above results, 160 °C, 3 MPa, 3:7 for the ratio of methanol to DMF, 40 g $L^{-1}$ for Cu-Mn concentration and 30 g $L^{-1}$ for CaO-$ZrO_2$ concentration are the optimum reaction variables to directly synthesize MF from syngas in liquid phase. Under this reaction conditions, the highest catalytic activity and MF

selectivity can be obtained over Cu-Mn/Ca-Zr catalyst. The catalytic performance of Cu-Mn/Ca-Zr catalyst is listed and compared to those of previous literatures in Table 2. As can be seen in Table 2, the CO conversion of 22.4% and the MF selectivity of 82.3% could be obtained on Cu-Mn/Ca-Zr catalyst under the optimum reaction conditions in this work. Although a relatively low CO conversion is presented on Cu-Mn/Ca-Zr compared to $NaOCH_3$/Cu-catalyst, HCOOK/Cu-catalyst and $KOCH_3/Ni(CO)_4$ in previous literatures,[49-51] Cu-Mn/Ca-Zr has higher MF selectivity than traditional catalysts above, which is due to the presence of synergistic effect between Cu-Mn and $CaO\text{-}ZrO_2$ samples.

### 3.4 Roles of $CaO\text{-}ZrO_2$ and Cu-Mn in MF synthesis

It is worth noticing that CO conversion and MF selectivity are extremely low when $CaO\text{-}ZrO_2$ or Cu-Mn catalyst is absence from liquid phase, as shown in Fig. 10, 11. However, they sharply increase when the $CaO\text{-}ZrO_2$ or Cu-Mn catalyst is introduced in system, indicating that both $CaO\text{-}ZrO_2$ and Cu-Mn catalysts play important roles in MF direct synthesis from syngas. Higher catalytic activity could be obtained when the concentration of $CaO\text{-}ZrO_2$ and Cu-Mn catalysts is 30 g $L^{-1}$ and 40 g $L^{-1}$ respectively, which might be due to the existence of synergistic effect between $CaO\text{-}ZrO_2$ and Cu-Mn samples. Two steps of reaction route might present in the direct synthesis of MF on Cu-Mn/Ca-Zr catalytic system, and different elementary reactions proceed on $CaO\text{-}ZrO_2$ and Cu-Mn catalysts, respectively (see 3.5). An optimum catalytic activity and MF selectivity can be obtained while two elementary reactions on $CaO\text{-}ZrO_2$ and Cu-Mn catalysts proceed synergistically.

$CaO\text{-}ZrO_2$ is a strong basic catalyst and can be applied to amounts of base-catalyzed reactions, such as Knoevenagel reaction, Michael additions, Tischenko

reaction, Claisen-Schmidt condensation and acetonylacetone cyclization. With the presence of mesoporous CaO-$ZrO_2$ solid base, Cu-Mn/Ca-Zr catalyst has an optimum catalytic activity in the synthesis of MF from syngas. The mesoporous structure and high specific surface of CaO-$ZrO_2$ make the basic sites expose on the surface of sample, and its basic property is beneficial to the synthesis of MF according to the previous literature.[52] The specifically proofs will be provided in another article of authors. On the other side, incomplete spinel of $Cu_{1.5}Mn_{1.5}O_4$ is formed in Cu-Mn oxide, in which two Jahn-Teller ions of $Cu^{2+}$ and $Mn^{3+}$ are presented and confirmed by XPS, leading to a large number of surface oxygen on Cu-Mn catalyst.[53] In addition, a strong interaction exists between Cu and Mn cations due to the formation of $Cu_{1.5}Mn_{1.5}O_4$ phase. Therefore, two factors of Cu-Mn mixed oxides mentioned above provide well catalytic activity and MF selectivity for direct MF synthesis from syngas over Cu-Mn/Ca-Zr catalyst.

### 3.5 Understanding of MF synthesis

In the traditional direct synthesis of MF, carbonylation and hydrogenation reaction mechanism has been generally accepted.[22-26] However, in this work, a new catalyst system of Cu-Mn/Ca-Zr is used, and different products are formed besides MF; thus the reaction mechanism might differ from carbonylation and hydrogenation. Basing on the results of Fig.10 and Fig. 11, it can be known that CaO-$ZrO_2$ or Cu-Mn catalysts are indispensable in the direct synthesis of MF to obtain high CO conversion and MF selectivity, and two elementary reactions on CaO-$ZrO_2$ and Cu-Mn catalysts proceed synergistically. According to the previous literatures,[30,54] the following reaction mechanism might exist in direct synthesis of MF on Cu-Mn/Ca-Zr catalyst, as shown in Fig. 12. At first adsorption formate species are formed on Cu-Mn catalyst,

and then the reaction between adsorption fromate species on Cu-Mn catalyst and methoxide adsorbed on CaO-$ZrO_2$ catalyst proceeds to produce methyl formate, at last partial methyl formate may hydrogenate with hydrogen atom on Cu-Mn catalyst to get methanol, which also illustrates the significant of synergism between Cu-Mn and CaO-$ZrO_2$. However, this reaction mechanism badly needs to be further confirmed in later work. We can conclude from above reaction route that the methanol in this system is not only a solvent but an intermediate to synthesize MF also.

## 4. Conclusions

Cu-Mn/Ca-Zr catalyst prepared by mechanical mixing Cu-Mn and CaO-$ZrO_2$ are highly active to the formation of methyl formate from syngas. Its methyl formate selectivity is higher than that of traditional catalyst (e.g. Cu-catalyst and $NaOCH_3$ ). Incomplete spinel of $Cu_{1.5}Mn_{1.5}O_4$ phase is formed in Cu-Mn mixed oxides, and CaO-$ZrO_2$ solid base exhibits mesoporous structure with three basic sites on the surface. The optimum reaction conditions for methyl formate synthesis are 160 ℃, 3 MPa, 3:7 for the ratio of methanol to DMF, 40 g $L^{-1}$ for Cu-Mn concentration and 30 g $L^{-1}$ for CaO-$ZrO_2$ concentration. Under this optimum reaction conditions, CO conversion of 22.4 % and MF selectivity of 82.3% are obtained, which can be attributed to the presence synergistic effect between Cu-Mn and CaO-$ZrO_2$ samples. The present work prepared a novel Cu-Mn/Ca-Zr combined catalyst, which seems great potential in the green and efficient route to synthesize methyl formate from syngas.

## Acknowledgements

The authors acknowledge the financial support from the National Natural Science Foundation of China (No. 21103217), the Strategic Priority Research Program of the Chinese Academy of Sciences (No. XDA01020304).

**References**

1 F. E. Celik, H. Lawrence, A. T. Bell, J. Mol. Catal. A: Chem., 2008, 288, 87.

2 K. B. Wang, G. Y. Wang, Chin. Chem. Lett., 2007, 18, 811.

3 K. Wang, J. Yao, Y. Wang, G. Wang, J. Nat. Gas Chem., 2007, 16, 286.

4 W. G. Huang, D. H. He, J. Y. Liu, Q. M. Zhu, Appl. Catal., A, 2000, 199, 93.

5 V. V. Kaichev, G. Y. Popova, Y. A. Chesalov, A. A. Saraev, D. Y. Zemlyanov, S. A. Beloshapkin, A. Knop-Gericke, R. Schloegl, T. V. Andrushkevich, V. I. Bukhtiyarov, J. Catal., 2014, 311, 59.

6 K. O. Adebowale, A. Adewuyi, K. D. Ajulo, Int. J. Green Energy, 2012, 9, 297.

7 T. Tsoncheva, T. Venkov, M. Dimitrov, C. Minchev, K. Hadjiivanov, J. Mol. Catal. A: Chem., 2004, 209, 125.

8 L. He, H. Liu, C. Xiao, Y. Kou, Green Chem., 2008, 10, 619.

9 Y. Iwase, T. Kobayashi, K. Inazu, A. Miyaji, T. Baba, Catal. Lett., 2007, 118, 146.

10 S. Jali, H. B. Friedrich, G. R. Julius, J. Mol. Catal. A: Chem., 2011, 348, 63.

11 G. T. Whiting, S. A. Kondrat, C. Hammond, N. Dimitratos, Q. He, D. J. Morgan, N. F. Dummer, J. K. Bartley, C. J. Kiely, S. H. Taylor, G. J. Hutchings, ACS Catal., 2015, 5, 637.

12 J. C. Colmenares, P. Lisowski, D. Lomot, O. Chernyayeva, D. Lisovytskiy, ChemSusChem 2015, 8, 1676.

13 R. Wang, Z. Wu, G. Wang, Z. Qin, C. Chen, M. Dong, H. Zhu, W. Fan, J. Wang,

RSC Adv., 2015, 5, 44835.

14 H. Huang, W. Li, H. Liu, Catal. Today, 2012, 183, 58.

15 C. Han, X. Yang, G. Gao, J. Wang, H. Lu, J. Liu, M. Tong, X. Liang, Green Chem., 2014, 16, 3603.

16 R. Wojcieszak, M. N. Ghazzal, E. M. Gaigneaux, P. Ruiz, Catal. Sci. Technol., 2014, 4, 738.

17 R. Wang, Z. Wu, C. Chen, Z. Qin, H. Zhu, G. Wang, H. Wang, C. Wu, W. Dong, W. Fan, J. Wang, Chem. Commun., 2013, 49, 8250.

18 M. Yadav, J. C. Linehan, A. J. Karkamkar, E. van der Eide, D. J. Heldebrant, Inorg. Chem., 2014, 53, 9849.

19 J. Chen, F. Xin, X. Yin, T. Xiang, Y. Wang, RSC Adv., 2015, 5, 3833.

20 J. Chen, S. Qin, G. Song, T. Xiang, F. Xin, X. Yin, Dalton Trans., 2013, 42, 15133.

21 J. Chen, F. Xin, S. Qin, X. Yin, Chem. Eng. J., 2013, 230, 506.

22 V. M. Palekar, J. W. Tierney, I. Wender, Appl. Catal., A, 1993, 103, 105.

23 V. M. Palekar, H. Jung, J. W. Tierney, Appl. Catal., A, 1993, 102, 13.

24 G. Jenner, Appl. Catal., A, 1995, 121, 25.

25 E. S. Lee, K. Aika, J. Mol. Catal. A: Chem., 1999, 141, 241.

26 S. Ohyama, E. S. Lee, K. Aika, J. Mol. Catal. A: Chem., 1999, 138, 305.

27 J. Lee, J. Kim, Y. Kim, Appl. Catal., 1990, 57, 1.

28 Y. Chen, B. Liaw, B. Chen, Appl. Catal., A, 2002, 236, 121.

29 R. Yang, X. Yu, Y. Zhang, W. Li, N. Tsubaki, Fuel, 2008, 87, 443.

30 Y. Zhang, R. Yang, N. Tsubaki, Catal. Today, 2008, 132, 93.

31 N. Tsubaki, M. Ito, K. Fujimoto, J. Catal., 2001, 197, 224.

32 B. Hu, K. Fujimoto, Appl. Catal., A, 2008, 346, 174.

33 Y. Liu, J. Chen, Y. Sun, Stud. Surf. Sci. Catal., 2005, 156, 249.

34 X. H. Zhang, H. Q. Su, Z. X. Yang, J. Mol. Catal. A: Chem., 2012, 360, 16.

35 S. Liu, J. Ma, L. Guan, J. Li, W. Wei, Y. Sun, Microporous Mesoporous Mater., 2009, 117, 466.

36 S. Xia, X. Guo, D. Mao, Z. Shi, G. Wu, G. Lu, RSC Adv., 2014, 4, 51688.

37 H. Cao, X. Li, Y. Chen, M. Gong, J. Wang, J. Rare Earths, 2012, 30, 871.

38 H. Y. Chen, D. J. Hsu, J. Alloys Compd., 2014, 598, 23.

39 B. Gillot, S. Buguet, E. Kester, C. Baubet, P. Tailhades, Thin Solid Films, 1999, 357, 223.

40 J. Papavasiliou, G. Avgouropoulos, T. Ioannides, J. Catal., 2007, 251, 7.

41 A. Wollner, F. Lange, H. Schmelz, H. Knozinger, Appl. Catal., A, 1993, 94, 181.

42 M. H. Kim, K. H. Cho, C. H. Shin, S. E. Kang, S. W. Ham, Korean J. Chem. Eng., 2011, 1139.

43 D. Fang, J. Xie, D. Mei, Y. Zhang, F. He, X. Liu, Y. Li, RSC Adv., 2014, 4, 25540.

44 G. Jernigan, G. A. Somorjai, J. Catal., 1994,147, 567.

45 G. Zhang, J. Long, X. Wang, W. Dai, Z. Li, L. Wu, X. Fu, New J. Chem., 2009, 33, 2044.

46 S. Y. Lee, N. Mettlach, N. Nguyen, Y. M. Sun, J. M. White, Appl. Surf. Sci., 2003, 206: 102.

47 H. Wang, M. Wang, W. Zhang, N. Zhao, W. Wei, Y. Sun, Catal. Today, 2006, 115, 107.

48 W. Chen, J. Nat. Gas Chem., 2000, 9, 139.

49 X. Liu, W. Chen, Y. Wu, Z. Jia, S. Luo, S. Li, Y. Yang, Z. Yu, J. Nat. Gas Chem., 1999, 8, 286.

50 S. Ohyama, Top. Catal., 2003, 22, 337.

51 B. Hu, K. Fujimoto, Appl. Catal., A, 2008, 346, 174.

52 S. Goodarznia, K. J. Smith, J. Mol. Catal. A: Chem., 2010, 320, 1.

53 H. Y. Chen, D. J. Hsu, J. Alloys Compd., 2014, 598, 23.

54 B. Hu, K. Fujimoto, Appl. Catal., B, 2010, 95, 208.

Table 1 Influence of methanol/DMF ratios on catalytic performance

| V ($CH_3OH$) : V (DMF) | Conv.CO | STY (g $L^{-1}$ $h^{-1}$) | Selectivity (%) | | | |
|---|---|---|---|---|---|---|
| | | MF | HCHO | MF | $C_2H_5OH$ | $CO_2$ |
| 9:1 | 10.9 | 0.67 | 17.4 | 42.1 | 30.0 | 10.5 |
| 7:3 | 13.8 | 0.75 | 15.7 | 50.9 | 22.8 | 10.6 |
| 5:5 | 12.4 | 4.09 | 4.0 | 80.6 | 11.3 | 4.1 |
| 3:7 | 11.9 | 4.18 | 1.7 | 83.5 | 11.0 | 3.8 |
| 1:9 | 7.5 | 2.44 | 2.0 | 83.8 | 11.8 | 2.5 |

Catalyst: C ($CaO-ZrO_2$) = 30 g $L^{-1}$, C (Cu-Mn) = 15 g $L^{-1}$, p = 4 MPa, T = 160 °C, t = 8 h, solvent: V = 50 mL.

Table 2 Catalytic performance of different catalysts

| Catalyst | Conv. CO (%) | Sel. MF (%) | Reference |
|---|---|---|---|
| Cu-Mn/Ca-Zr | 22.4 | 82.3 | This work[a] |
| $Ni(CO)_4$, $KOCH_3$ | 57.7 | 66.9 | 26 |
| Cu-Mn, $NaOCH_3$ | - | 73.2 | 49 |
| CuCl, $NaOCH_3$ | - | 40.3 | 49 |
| Cu-Cr, $KOCH_3$ | 88.6 | 5.6 | 50 |
| HCOOK, Cu catalyst | 75.6 | 2.6 | 51 |

[a] C ($CaO-ZrO_2$) = 30 g $L^{-1}$, C (Cu-Mn) = 40 g $L^{-1}$, p = 3 MPa, T = 160 °C, t = 8 h, solvent: V ($CH_3OH$) = 15 mL, V (DMF) = 35 mL.

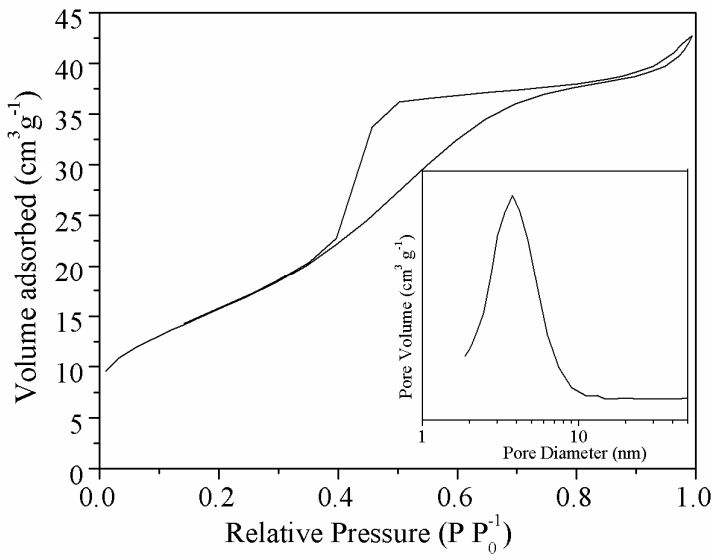


Fig. 1 $N_2$ isotherm adsorption-desorption and pore size distribution (inserted) profiles of CaO-$ZrO_2$

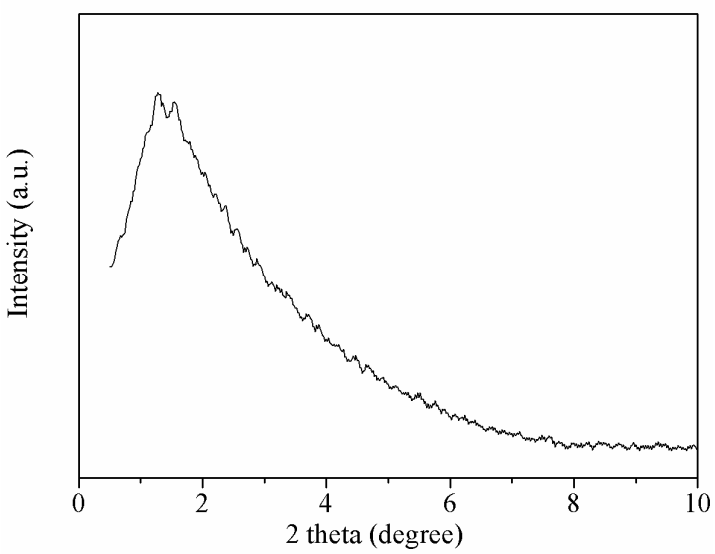


Fig. 2 SXRD plot of CaO-$ZrO_2$ catalyst

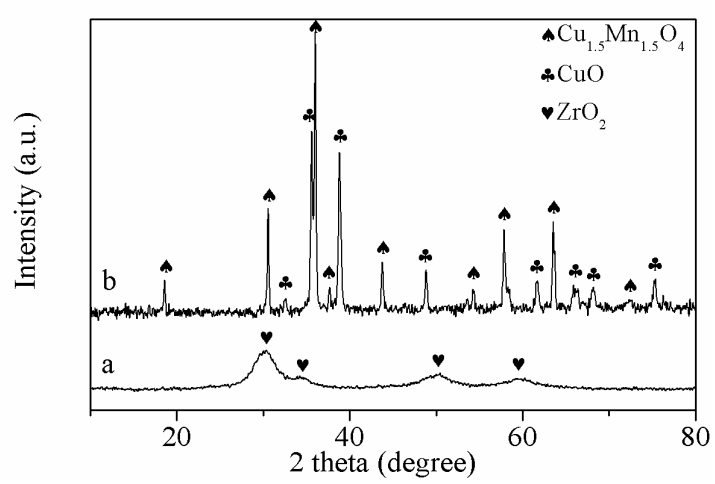


Fig. 3 XRD patterns of $CaO\text{-}ZrO_2$ (a) and Cu-Mn (b) catalysts

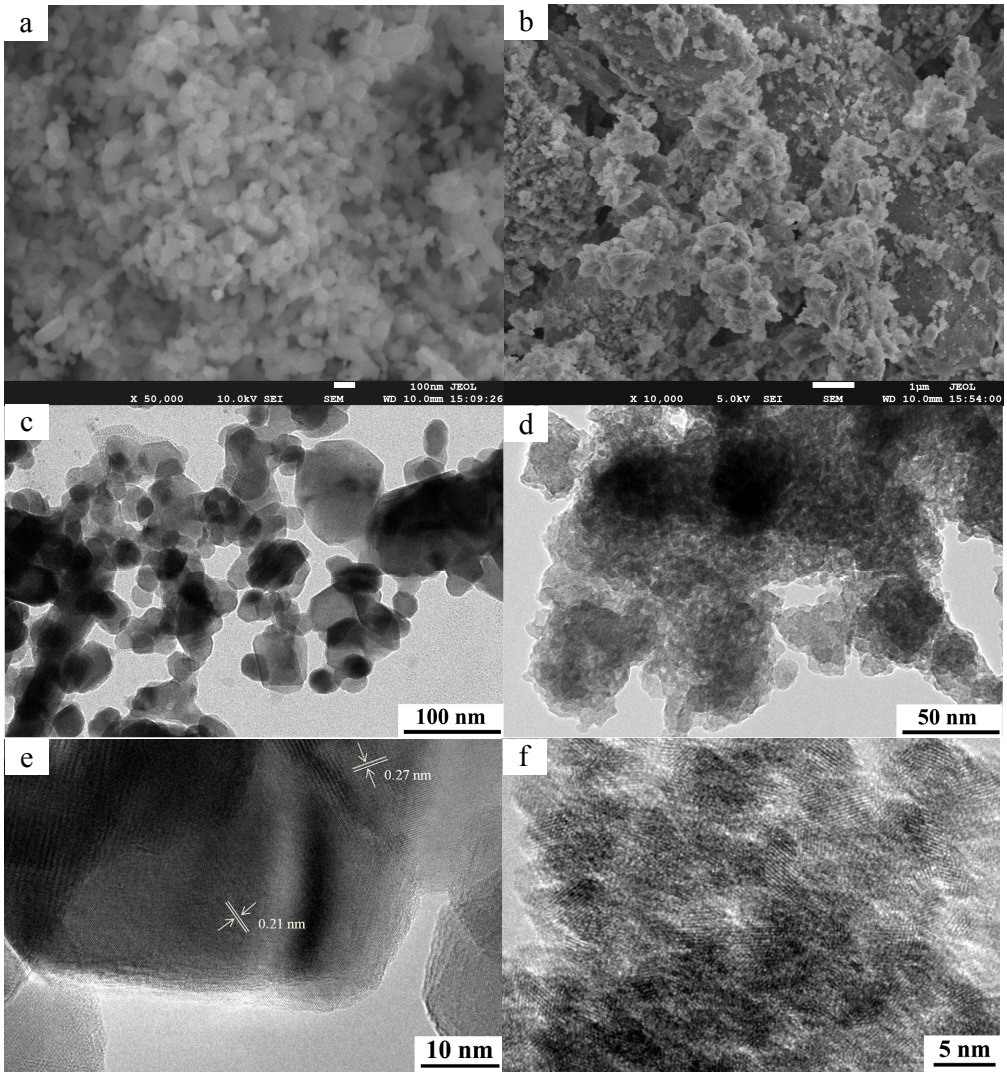


Fig. 4 SEM (a, b) and TEM (c-f) images of the Cu-Mn (a, c, e) and CaO-$ZrO_2$ (b, d, f) catalysts

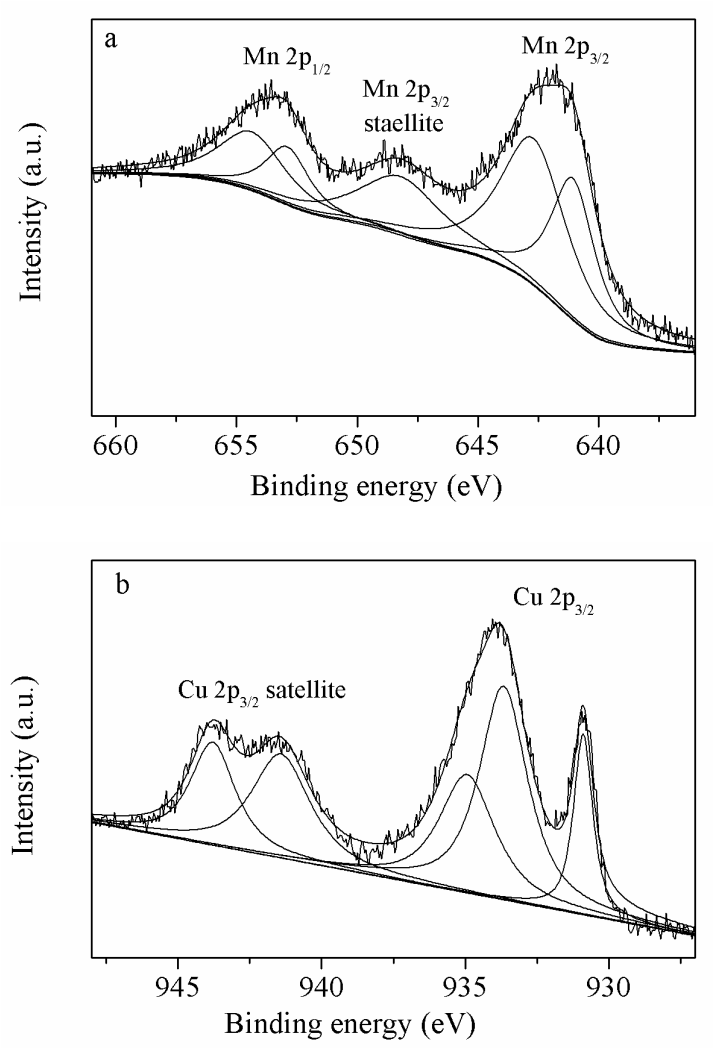


Fig. 5 Mn 2p (a) and Cu 2p (b) XPS of the Cu-Mn catalyst

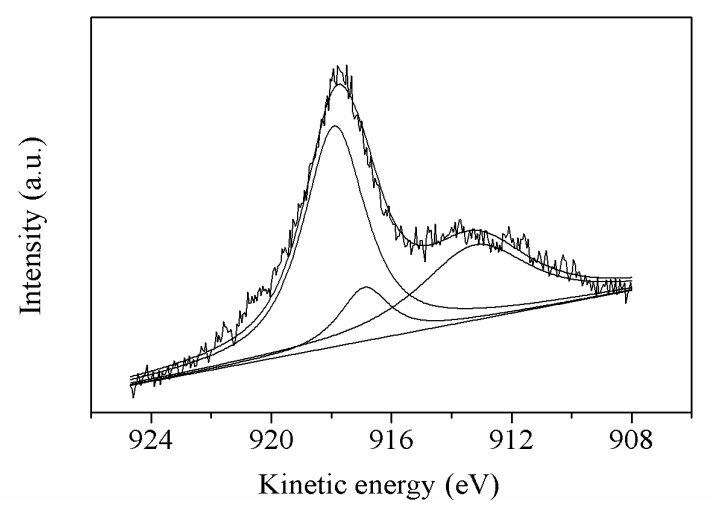


Fig. 6 XPS of Cu $L_3MM$ Auger electron of Cu-Mn catalyst

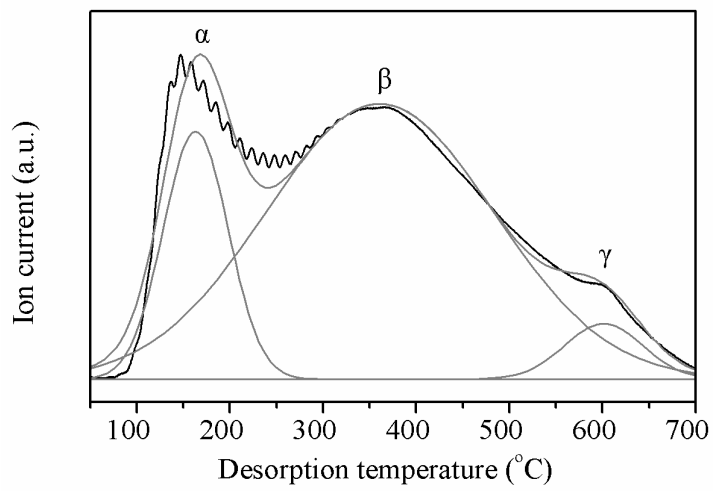


Fig. 7 $CO_2$-TPD plot of CaO-$ZrO_2$ catalyst

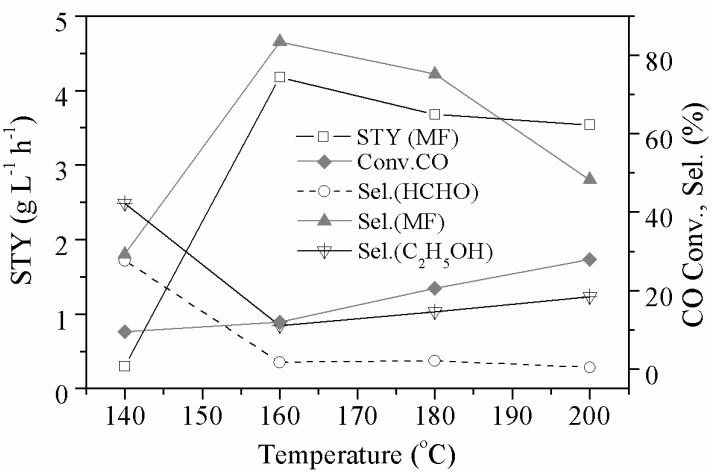


Fig. 8 The influence of reaction temperature on catalytic performance

Catalyst: C (CaO-$ZrO_2$) = 30 g $L^{-1}$, C (Cu-Mn) = 15 g $L^{-1}$, p = 4 MPa, t = 8 h, solvent: V ($CH_3OH$) = 15 mL, V (DMF) = 35 mL.

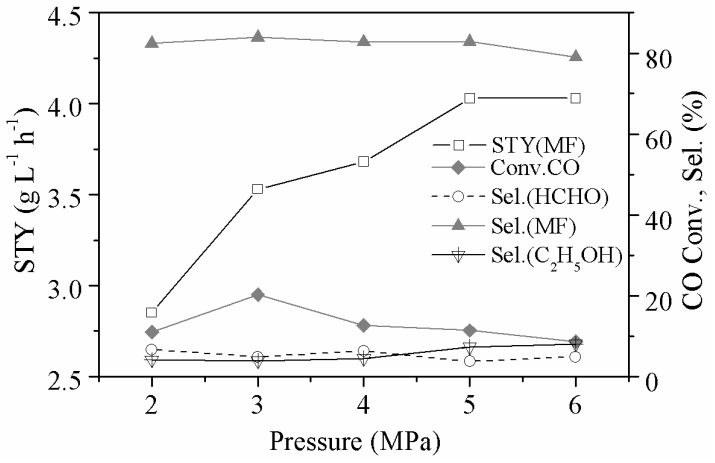


Fig. 9 The influence of reaction pressure on catalytic performance

Catalyst: C (CaO-$ZrO_2$) = 30 g $L^{-1}$, C (Cu-Mn) = 15 g $L^{-1}$, T = 160 °C, t =8 h, solvent: V ($CH_3OH$) = 15 mL, V (DMF) = 35 mL.

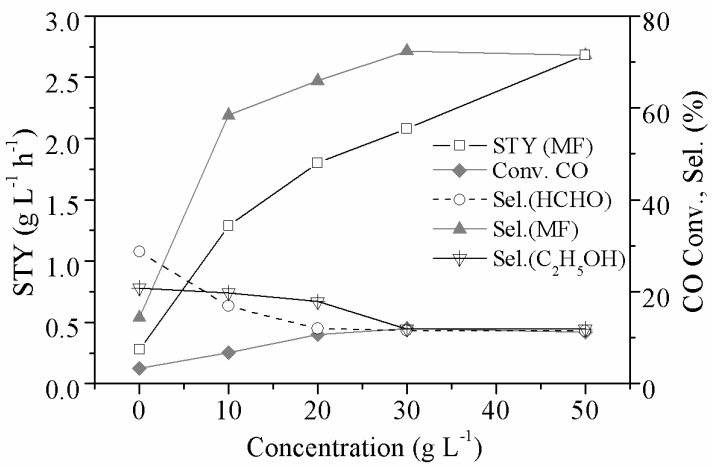


Fig. 10 Influence of $CaO\text{-}ZrO_2$ concentration on catalytic performance

Catalyst: C (Cu-Mn) = 15 g $L^{-1}$, p = 4 MPa, T = 160 °C, t= 8 h, solvent: V ($CH_3OH$) = 15 mL, V (DMF) = 35 mL.

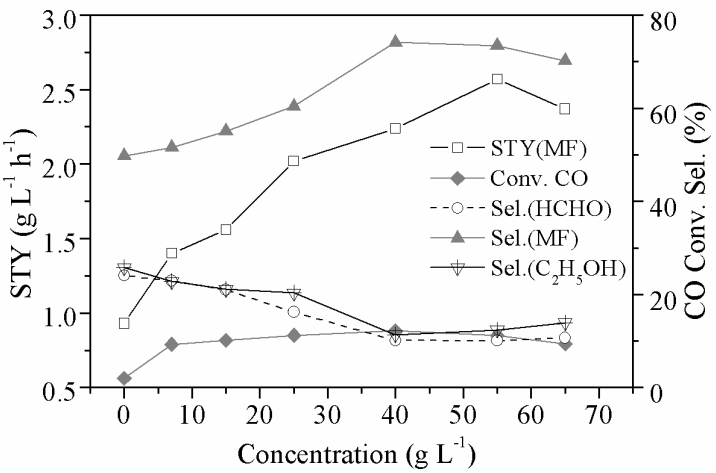


Fig. 11 Influence of Cu-Mn concentration on catalytic performance

Catalyst: C ($CaO\text{-}ZrO_2$) = 20 g $L^{-1}$, p = 4 MPa, T = 160 °C, t = 8 h, solvent: V ($CH_3OH$) = 15 mL, V (DMF) = 35 mL.

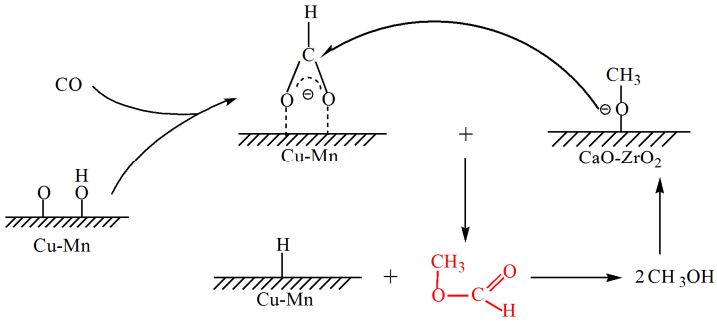


Fig. 12 Schematic for MF direct synthesis over Cu-Mn/Ca-Zr catalyst

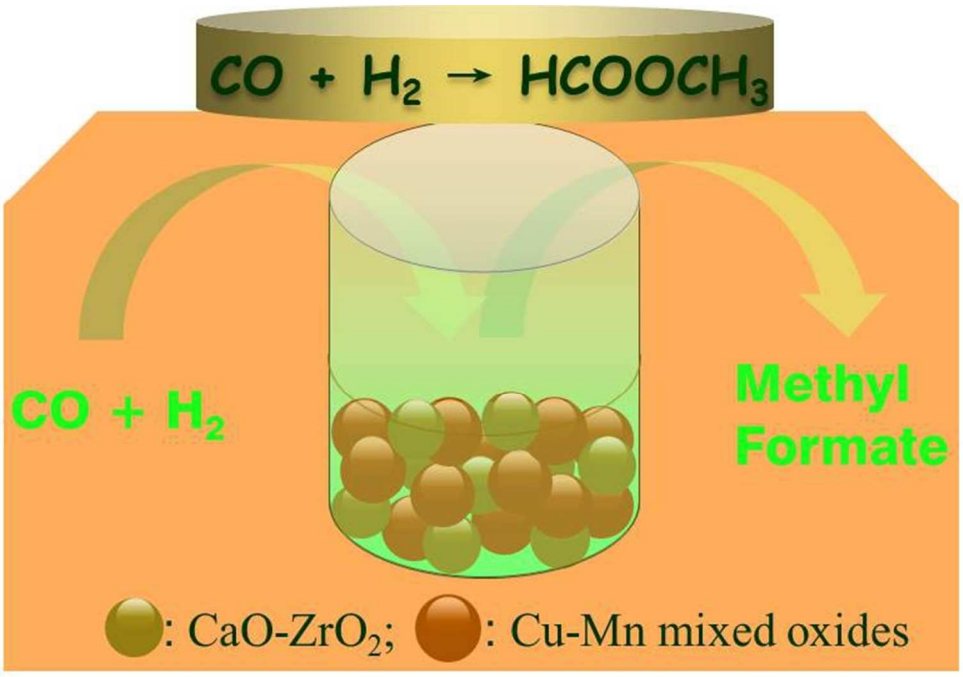


135x92mm (150 x 150 DPI)